Developmental Biology 332 (2009) 273–286

Contents lists available at ScienceDirect

Developmental Biology

journal homepage: www.elsevier.com/developmentalbiology

Analysis of early nephron patterning reveals a role for distal RV proliferation in fusion to the ureteric tip via a cap mesenchyme-derived connecting segment

Kylie Georgas [a], Bree Rumballe [a], M. Todd Valerius [b], Han Sheng Chiu [a], Rathi D. Thiagarajan [a], Emmanuelle Lesieur [a], Bruce J. Aronow [c], Eric W. Brunskill [d], Alexander N. Combes [a], Dave Tang [a], Darrin Taylor [a], Sean M. Grimmond [a], S. Steven Potter [d], Andrew P. McMahon [b], Melissa H. Little [a,*]

[a] NHMRC Principal Research Fellow, Institute for Molecular Bioscience, The University of Queensland, St Lucia, 4072, Australia
[b] Department of Molecular and Cellular Biology, Harvard University, 16 Divinity Avenue, Cambridge, MA 02138, USA
[c] Division of Biomedical Informatics, Children's Hospital Medical Center, 3333 Burnet Ave, Cincinnati, OH 45229, USA
[d] Division of Developmental Biology, Children's Hospital Medical Center, 3333 Burnet Ave, Cincinnati, OH 45229, USA

ARTICLE INFO

Article history:
Received for publication 17 April 2009
Revised 28 May 2009
Accepted 29 May 2009
Available online 6 June 2009

Keywords:
Renal vesicle
Nephron development
Gene expression
Renal connecting tubule formation
Nephron patterning

ABSTRACT

While nephron formation is known to be initiated by a mesenchyme-to-epithelial transition of the cap mesenchyme to form a renal vesicle (RV), the subsequent patterning of the nephron and fusion with the ureteric component of the kidney to form a patent contiguous uriniferous tubule has not been fully characterized. Using dual section in situ hybridization (SISH)/immunohistochemistry (IHC) we have revealed distinct distal/proximal patterning of Notch, BMP and Wnt pathway components within the RV stage nephron. Quantitation of mitoses and Cyclin D1 expression indicated that cell proliferation was higher in the distal RV, reflecting the differential developmental programs of the proximal and distal populations. A small number of RV genes were also expressed in the early connecting segment of the nephron. Dual ISH/IHC combined with serial section immunofluorescence and 3D reconstruction revealed that fusion occurs between the late RV and adjacent ureteric tip via a process that involves loss of the intervening ureteric epithelial basement membrane and insertion of cells expressing RV markers into the ureteric tip. Using *Six2-eGFPCre*×*R26R-lacZ* mice, we demonstrate that these cells are derived from the cap mesenchyme and not the ureteric epithelium. Hence, both nephron patterning and patency are evident at the late renal vesicle stage.
© 2009 Elsevier Inc. All rights reserved.

Introduction

The nephron is the functional unit of the postnatal kidney. Humans possess anywhere between 300,000 and 1.8 million nephrons per kidney and all of these nephrons are endowed by 36 weeks of gestation (Hoy et al., 2008; Nyengaard and Bendtsen, 1992). This variability in nephron number reflects the fact that the process of nephron endowment can be dramatically affected in utero by both environmental and genetic factors. While the inverse relationship between nephron number and renal failure during postnatal life is now well appreciated (Brenner and Chertow, 1994; Brenner et al., 1988; Brenner and Milford, 1993; Mackenzie et al., 1994), the precise molecular basis of nephron induction and patterning remains to be fully defined.

The process of nephrogenesis involves reciprocal interactions between two tissues that share a common cellular origin from a population within the intermediate mesoderm (Mugford et al., 2008), the metanephric mesenchyme and the ureteric bud. Around the tip of the branching ureteric bud, the metanephric mesenchyme condenses to form the cap mesenchyme. The cells of the cap mesenchyme are progenitor cells which self renew throughout kidney development to supply the cells required for nephron induction. The process of nephron induction requires a mesenchyme to epithelial transition (MET). Here, cells of the cap mesenchyme in a specific location proximal to the ureteric tip and immediately adjacent to its basement membrane condense to form a ball of cells termed the pretubular aggregate. This process is dependant on *Wnt9b* expression from the ureteric epithelium, which acts as the earliest inducer of MET (Carroll et al., 2005). Lineage tracing has determined that it is from the cap mesenchyme via the RV that all epithelial components of the nephron arise including the renal tubules and parietal and visceral epithelia of the renal corpuscle, with the exception of the collecting ducts which are derived from the ureteric bud (Kobayashi et al., 2008a; Oxburgh et al., 2004).

Formation of a mature nephron requires segmentation and patterning (Dressler, 2006; Kopan et al., 2007). Clear segmentation of the early nephron is readily distinguishable by the S-shaped body stage which is organized into distinct connecting, distal, medial and proximal segments, and where the cells of the proximal segment have further differentiated to form two distinct epithelia, the parietal (Bowman's capsule) and visceral (podocyte layer) epithelium of the

* Corresponding author. Fax: +1 617 3346 2101
E-mail address: m.little@uq.edu.au (M.H. Little).

0012-1606/$ – see front matter © 2009 Elsevier Inc. All rights reserved.
doi:10.1016/j.ydbio.2009.05.578

future renal corpuscle. These distal–proximal segments are identifiable by restricted expression of the molecular markers E-cadherin, Cadherin-6, Jag1, Wt1 and Pax2 (Dressler, 2006). At the earlier comma-shaped body stage, the nephron can also be divided into distal (upper limb) and proximal (lower limb) portions and there is some evidence of segmentation/polarization as early as the RV stage (Kopan et al., 2007). This was first reported for specific cadherins, with Cadherin-6 expression observed to be restricted to the proximal RV and E-cadherin to the distal RV (Cho et al., 1998; Mah et al., 2000). *Pou3f3* and *Dll1* display strong restricted gene expression in the distal RV (Kobayashi et al., 2005; Nakai et al., 2003) and we have shown that the Wt1 protein is a marker of the proximal RV (Georgas et al., 2008).

As well as segmentation, formation of a functional nephron requires fusion to the ureteric bud. The literature generally regards this fusion event to occur fairly early in nephron formation, with reports stating that a connection is viable at the S-shaped body stage. In contrast, Bard et al. (2001) proposed that fusion with the ureteric bud occurs at the RV stage. The cellular origin of this link between the RV and the tip of the UB, the connecting segment, has not been determined, nor has the molecular and cellular basis of the fusion event. However, *Cdh6* (Cadherin-6) mutant mice show altered RV polarization and a consequent delay in MET. This delay is thought to affect the fusion of the early nephron to the ureteric tip as a significant portion of nephrons fail to fuse. The resultant non-functional nephrons necrose after birth leading to a signification reduction in nephron number in the adult (Mah et al., 2000). *Cdh4* (Cadherin-4) mutant mice display a similar phenotype to the *Cdh6* mice with slightly reduced early nephron numbers and subtle changes to the proximal tubules (Dahl et al., 2002). Despite these examples, overall the molecular basis and role of proximal–distal patterning and fusion of the RV are poorly understood and the genes involved are only beginning to emerge.

In this study, we sought to further analyze the molecular basis of RV patterning and the timing and mechanism of fusion via careful spatial and temporal analyses of gene and protein expression across the different stages of nephrogenesis. These analyses give a direct insight into the genes involved in the early events of nephron patterning and fusion and identify novel genes showing polarized gene expression in the early RV. With respect to timing, this fusion event begins at the late renal vesicle (syn: connected RV) stage. The 3D modeling and analysis of basement membrane dynamics also reveals the complex relationships between new forming and existing nephrons within the nephrogenic zone and highlights the spatial arrangement of the basement membrane during fusion. We report preferential proliferation of distal RV cells, which may drive the process of fusion, and also show using lineage tracing that the connecting segment is derived from the RV and not the ureteric tip. These results lay the detailed foundation for the dissection of processes involved in early nephron patterning and fusion and provide a framework upon which to examine defects in these critical early events in mutant animals.

Materials and methods

Microarray analysis

Genes upregulated in the renal vesicle were identified by performing a three-way comparison between the expression profiles of laser captured 15.5 dpc collecting duct, 12.5 dpc renal vesicle (RV) and 15.5 dpc S-shaped body, generated as part of GUDMAP (Brunskill et al., 2008). The entire dataset is available from NCBI via the GEO database (accession number GSE6290) and on the GUDMAP database http://www.gudmap.org. The compiled expression data was RMA normalized in Genespring Version 7.3 (Agilent) and 1 way ANOVA ($P<0.005$) with Benjamini–Hochberg correction for FDR performed to identify differentially expressed probes for all three dissected compartments. By these criteria 379 genes were upregulated in the RV. Finally, the candidate RV gene list was further restricted to those genes ($n=63$) that were previously reported to be downregulated in the developing kidneys of Wnt4 knock out versus wild-type mice (NCBI accession number GSE6934) (Valerius and McMahon, 2008). Throughout this manuscript, MGI (Mouse Genome Informatics) gene symbols have been used. The complete list of probes identified from the microarray analysis, with Affymetrix Identifier, gene symbol and descriptions are shown in Supplementary Table S1 (available at http://grimmond.imb.uq.edu.au/gudmap/supplementaryData/index.html).

Tissue collection and processing

Adult pregnant female outbred CD1 mice were sacrificed by cervical dislocation and the embryos harvested at 10.5 dpc (TS17), 13.5 dpc (TS21) and 15.5 dpc (TS23). A normal variation of ± 0.5 days was observed in the stage of the embryos. For all procedures, dissected tissues were fixed in 4% paraformaldehyde (PFA) in PBS at 4 °C overnight. Tissues were dehydrated (methanol/PBTX for wholemount tissues; ethanol/water for sectioned tissues) and stored in alcohol (100% methanol at −20 °C for wholemount tissues; 70% ethanol at 4 °C for sectioned tissues). Paraffin-embedding and sectioning was performed as described recently by our laboratory (Rumballe et al., 2008).

In situ hybridization

The complete protocols for riboprobe generation, WISH, SISH and IHC from our laboratory are available on the GUDMAP website within *Research*, *Protocols* (http://www.gudmap.org/Research/Protocols/Little.html) and have been described previously (Georgas et al., 2008; Little et al., 2007; Rumballe et al., 2008). Digoxigenin (DIG)-labelled antisense riboprobes were generated by PCR followed by transcription. PCR primers were designed to amplify a 500–1000 bp 3′UTR region of each gene. Riborobes were amplified from either the FANTOM2 60 k cDNA library or whole 15.5 dpc embryonic mouse cDNA using two sequential rounds of PCR. In vitro transcription of DIG-labelled riboprobes was performed using T7 RNA Polymerase (Roche) utilizing a T7 polymerase promoter tag sequence within the reverse primer. Riboprobes were then purified using Roche Quick Mini Spin Columns and stored at −70 °C. The complete list of riboprobes generated, with PCR primer sequences and DNA probe identifiers are shown in Supplementary Table S1 (available at http://grimmond.imb.uq.edu.au/gudmap/supplementaryData/index.html).

Section in situ hybridization

Section in situ hybridization (SISH) was performed on 7 μm paraffin sectioned 15.5 dpc kidneys. Following dewaxing, the SISH process was performed using a Tecan Freedom Evo 150 robot (Little et al., 2007; Rumballe et al., 2008). Pre-hybridization treatments, hybridization of riboprobe, incubation with anti-DIG-alkaline phosphatase and all washes were performed in the robot. Hybridization was performed at 64 °C for 10 h with 0.3–0.5 μg/ml of probe in hybridization buffer (50% formamide, 10% dextran sulphate, 1× Denhardt's, 0.2 mg/ml yeast tRNA, 0.5 mg/ml salmon sperm, 2× SSC). Anti-DIG-alkaline phosphatase Fab fragments (1:2000, Roche) were incubated for 60 min at 25 °C. Slides were removed from the robot for the detection of alkaline phosphatase activity using the chromogenic substrate BM Purple. Once the signal had reached optimal intensity (4–60 h), the slides were rinsed and fixed in 4% PFA at 25 °C for 20 min then mounted in aqueous mounting medium.

Dual section in situ hybridization/immunohistochemistry

Dual SISH/IHC was performed in order to more accurately annotate the expression patterns of some genes by SISH and the procedure has been described previously (Georgas et al., 2008). The following antibodies were used; anti-Calbindin (Sigma, C9848), anti-Wt1 (DakoCytomation, 6F-H2), anti-collagen IV (Chemicon International, AB756P) and anti-laminin (Sigma, L9393). Briefly, following SISH tissues were blocked with 2% heat inactivated sheep serum in PBS for 1 h. Primary antibodies were used at dilutions of 1:100–1:250 and incubated overnight at 4 °C. Secondary biotin-conjugated antibodies (Zymed Laboratories, Inc.) were used at a 1:200 dilution and incubated for 1 h. Labeled proteins were visualized with horseradish peroxidase (VECTOR Laboratories VECTASTAIN Elite ABC Reagent, PK-6100) and DAB peroxidase substrate solution (VECTOR Laboratories DAB Substrate Kit for Peroxidase, SK-4100) for the appropriate development time (0.5–2 min). Sections were rinsed and fixed in 4% PFA at 25 °C for 20 min and mounted in aqueous mounting medium.

Photography of SISH and dual ISH/IHC and annotation of expression

Sectioned kidneys were scanned automatically using the semi-automated .slide System from Olympus and Soft Imaging Systems (BX51 microscope, digital CCD camera, motorized scanning stage and workstation, automated slide loader and .slide software) and representative images were captured using Olyvia software (Soft Imaging Systems, Olympus) and Adobe Photoshop CS2. Gene and protein expression patterns were annotated following standard procedures developed for GUDMAP using the published text-based anatomical ontology of the mouse urogenital system (Little et al., 2007) and are available on the GUDMAP database http://www.gudmap.org.

Quantitation of proliferating cells by phospho-Histone H3

Kidneys from 15.5 dpc embryos were sectioned at 7 μm through the mid-sagittal region of each kidney. Each section included nephrogenic zone, cortex and medulla. Immunohistochemistry using anti-phospho-Histone H3 (Ser10) antibody (Millipore, 06-570, 1:100) was performed after in situ hybridization to detect *Wnt4* mRNA using the dual SISH/IHC procedure described above. Kidney sections ($n=9$) from different embryos were evaluated by counting the number of cells staining positive for the phospho-Histone H3 antigen and noting the structure and nephron stage the positive cells were located in. The following structures were analyzed; whole kidney, ureteric tip ($n=209$), metanephric mesenchyme (nephrogenic interstitium and cap mesenchyme), pretubular aggregates ($n=108$), renal vesicles (RV, $n=61$), comma-shaped bodies (CB, $n=33$) and S-shaped bodies (SB, $n=35$). RV and CB were further divided into proximal and distal regions and SB into proximal, medial and distal segments. The structures and their sub-domains, which are illustrated in the schematic in Fig. 1B, were identified using anatomical histology and *Wnt4* gene expression.

Section immunofluorescence

Immunofluorescence was performed on paraffin-embedded 15.5 dpc kidneys sectioned through the mid-sagittal region. The following antibodies were used; anti-Calbindin (Sigma, C9848), anti-collagen IV (Chemicon International, AB756P), anti-laminin (Sigma, L9393), anti-E-cadherin (BD Biosciences, 610181, 612130) and anti-Cyclin D1 (Santa Cruz Biotechnology Inc., sc-450). Following standard dewaxing and rehydration to water, tissues were treated in an antigen unmasking procedure by boiling in Antigen Unmasking solution (H-3300 Vector Laboratories; 4.7:500 in water) using a microwave on high for 12 min. Tissues were left to cool, washed in PBS and blocked with 2% HISS/PBS for 1 h at room temperature. Primary antibodies were used at dilutions of 1:100 to 1:250 in 1% HISS/PBS and incubated overnight at 4 °C. Fluorescently labeled secondary antibodies (Molecular Probes) were used at a 1:200 dilution in 1% HISS/PBS for 1 h at room temperature. Nuclei were stained with DAPI (1:5000 in PBS) for 5 min, washed and mounted in aqueous mounting medium for fluorescence (Vectorshield). Tissues were photographed using a standard fluorescent microscope with 60× and 100× objectives (Olympus BX51, DP70 color 12 megapixel digital camera, Olympus Image Application Software and Adobe Photoshop CS2).

Wholemount immunofluorescence and confocal microscopy

Wholemount IF was performed using a procedure recently described for the mouse testis (Combes et al., 2009). Dissected kidneys from 15.5 dpc embryos which were cut in half with a scalpel blade either sagittally or transversely were fixed in 4% PFA overnight. Samples were blocked for 4 h in 10% HISS/PBTX and incubated with primary antibodies at 4 °C overnight. Samples were washed in PBTX and blocked again for 1–2 h, incubated with secondary antibodies overnight before washing thoroughly in PBTX. Antibodies and dilutions are identical to those used for section IF. Samples were mounted on single concave microscope slides (Sail) in 60% glycerol and imaged on a Zeiss LSM 510 META inverted confocal microscope. Image stacks were captured using 20× and 40× objectives every 1–2 μm for approximately 30 slices. Representative images and movies were generated using Zeiss LSM Image Browser software.

3D modeling of nephrons

For collection of data for modeling, section immunofluorescence and imaging was performed on serial 4 μm sagittal kidney sections using the procedure described above. Section images were manually aligned against images from adjacent sections using Adobe Photoshop CS2 and the aligned image layers were imported into the tomography program IMOD http://bio3d.colorado.edu/imod/ (Kremer et al., 1996). Individual nephrons and the ureteric tree were outlined in each section across the image layers then meshed together and rendered to create a 3D representation of the tissue structure in the sample. 2D representative images and 3D movies were created using IMOD software and Adobe ImageReady CS2.

Analysis of kidneys from Six2-TGC/R26R-lacZ mouse strain

Whole urogenital systems (UGS) at 15.5 dpc were dissected and fixed in 4% PFA for 2 h at 4 °C. UGS were embedded in OCT medium and frozen in a dry ice/ethanol bath. Mid-sagittal 30 μm cryosections were cut and mounted on coated slides, then stored at −80 °C until use. Room temperature sections were washed in PBT (PBS + 0.1% Triton), then blocked with 5% HISS/PBT for 1 h at room temperature. Primary antibodies were incubated on the sections in 1% HISS/PBT overnight at 4 °C, washed three times in PBT, then incubated with secondary antibodies in 1% HISS/PBT for 2 h. Following a final 3× wash in PBT, nuclei were stained with Hoechst stain (1:10,000 dilution in PBS), air-dried and coverslip mounted with Vectorshield. The antibodies used were mouse anti-Cytokeratin (Sigma, C2562) at 1:100, chicken anti-GFP (Aves Labs, GFP-1020) at 1:300, and mouse anti-Beta galactosidase (Cappel, 55976) at 1:20,000. Images were collected on a Zeiss LSM510 META confocal microscope.

Results

Selection of genes upregulated in the mouse renal vesicle

In order to investigate the molecular regulation of the renal vesicle more fully, we analyzed two different sets of existing microarray data

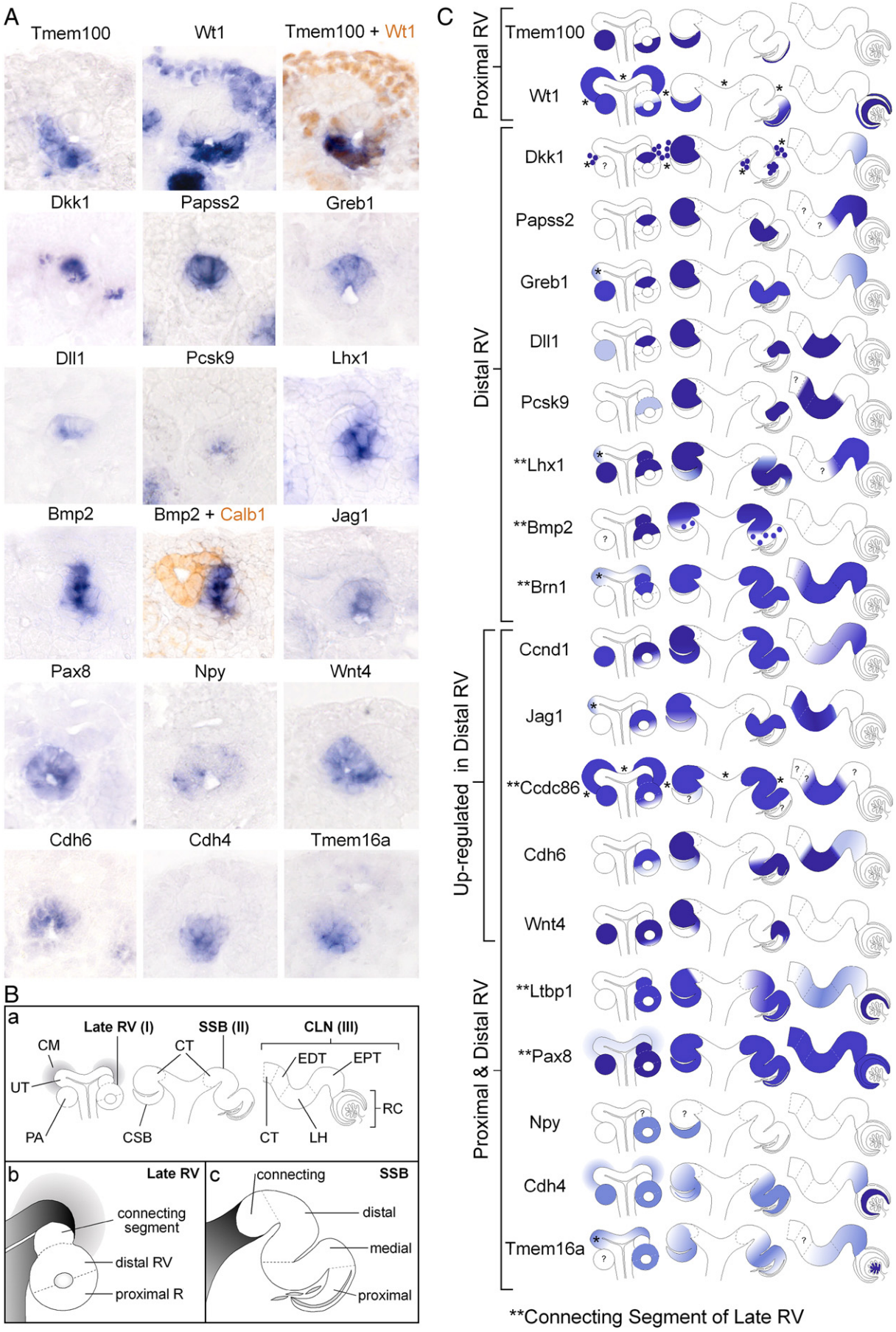
A
Tmem100
Wt1
Tmem100 + Wt1
Dkk1
Papss2
Greb1
Dll1
Pcsk9
Lhx1
Bmp2
Bmp2 + Calb1
Jag1
Pax8
Npy
Wnt4
Cdh6
Cdh4
Tmem16a
B
a
Late RV (I)
SSB (II)
CLN (III)
CM
CT
EDT
EPT
UT
RC
PA
CSB
CT
LH
b
Late RV
connecting segment
distal RV
proximal R
c
connecting
SSB
distal
medial
proximal
C
Proximal RV
Tmem100
Wt1
Distal RV
Dkk1
Papss2
Greb1
Dll1
Pcsk9
**Lhx1
**Bmp2
**Brn1
Up-regulated in Distal RV
Ccnd1
Jag1
**Ccdc86
Cdh6
Wnt4
Proximal & Distal RV
**Ltbp1
**Pax8
Npy
Cdh4
Tmem16a
**Connecting Segment of Late RV

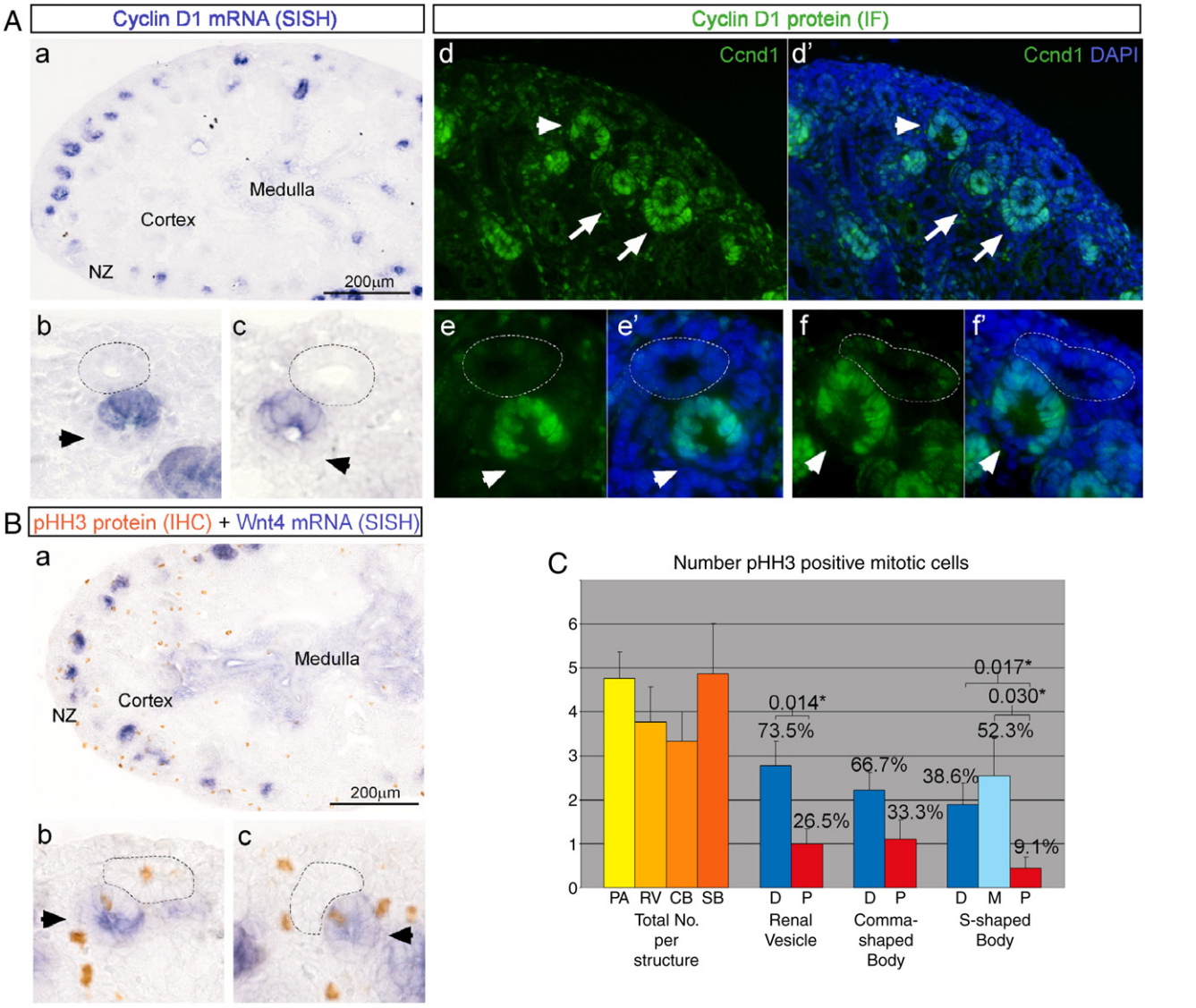

Fig. 2. Increased cell proliferation in the distal renal vesicle. The expression patterns of two markers of proliferation, Cyclin D1 (Ccnd1) — G1 phase and phospho-Histone H3 (pHH3) — mitosis, were analyzed in the sub-domains of renal vesicles (RV) and later stage nephrons in 15.5 dpc kidney sections. A. *Ccnd1* gene expression was examined by SISH. (a) *Ccnd1* expression was observed in early nephrons of the nephrogenic zone (NZ) and adjacent cortex and in medullary interstitial cells. (b, c) High magnification images of RVs show regional expression in the distal RV. (d–f) Expression of Ccnd1 protein by immunofluorescence shows an identical pattern to the gene. (d,d′) Ccnd1 in RVs (arrowheads) and later stage nephrons (arrows) in the cortex (60×). (e–f) High magnification shows expression in distal RV (100×). Gene and protein expression of Ccnd1 was either weak or not detected in the proximal RV (arrowheads in b, c, e, f). The ureteric tip is outlined. B. Mitotic cells were assessed using dual SISH/IHC with anti-pHH3 antibody (orange) and *Wnt4* gene expression (blue) to identify early nephrons. (a) Large numbers of mitotic cells were detected in the nephrogenic zone (NZ). (b, c) High magnification images of RVs (arrowheads) show a mitotic cell in the distal RV. The ureteric tip is outlined. C. Semi-quantitative analysis of the number of pHH3 positive mitotic cells relative to their location in the sub-domains of early nephrons showed increased mitosis in the distal nephron (error bars, SE). On left: Total No. per structure indicates whole nephron; PA, RV, CB, SB. On right: RV, CB and SB divided into D (distal), P (proximal) and M (medial) domains. Percentages and significance (*$P<0.05$) calculated by comparing the segments within each nephron stage. PA = pretubular aggregate ($n=108$), RV = renal vesicle ($n=61$), CB = comma-shaped body ($n=33$, SB = S-shaped body ($n=35$).

Fig. 1. Molecular subdivision of the renal vesicle and patterning in early nephrons. Section in situ hybridization (SISH) was performed on sagittal sections of 15.5 dpc kidneys to examine the spatial expression during nephron formation of genes upregulated in the renal vesicle (RV). (A) Examples of gene expression in the RV. Images are oriented with the outer edge of the kidney at the top. *Tmem100* and *Bmp2* are shown with dual IHC using anti-Wt1 and anti-Calbindin (ureteric tip) antibodies respectively. (B) (a) Schematic diagram of nephron formation showing nephrons from pretubular aggregate (PA) to capillary loop nephron (CLN) and adjacent kidney structures. The domains which divide the CSB, SSB and CLN are based on anatomical histology and have been described previously (Little et al., 2007). (b) Late RV stage is shown to indicate the sub-domains described here which are based on anatomical histology and gene expression. The proximal and distal RV domains divide the RV in half through the centre of the lumen and are oriented with respect to the location of the ureteric tip, where the distal RV is the half closest to the tip. (c) Sub-domains of the S-shaped body (SSB). CM = cap mesenchyme, UT = ureteric tip, CSB = comma-shaped body, CT = connecting tubule, EDT = early distal tubule, LH = anlage of Loop of Henle, EPT = early proximal tubule, RC = renal corpuscle. (C) Based on the SISH results at 15.5 dpc, the expression domains of each gene were painted onto the schematic of nephron stages. Expression strength is indicated by depth of blue color — light blue (weak) to dark blue (strong). Genes were divided into groups based on expression in the sub-domains of the RV; proximal, distal (restricted and upregulated) and non-polarized expression (proximal and distal). Genes which were upregulated in distal RV showed weaker expression in the proximal RV domain. **Genes with expression in the connecting segment of RV. *In the schematics, indicates the following; *Wt1*, *Ccdc86*, *Dkk1* — expression in nephrogenic and cortical interstitium (*Dkk1*-subset of interstitial cells; hence spotted expression); and *Greb1*, *Jag1*, *Pou3f3*, *Lhx1*, *Tmem16a* — expression detected in a subset of ureteric tips. ? = uncertain expression. (The expression patterns of these genes in maturing nephrons (IV) and other structures within the 15.5 dpc kidney are available on the GUDMAP website http://www.gudmap.org).

from embryonic mouse kidney (Brunskill et al., 2008; Valerius and McMahon, 2008) to select RV-enriched genes. Initially, a three-way comparison between renal vesicle, collecting duct and S-shaped body was performed. These structures were isolated using laser capture micro-dissection of wild-type embryonic kidneys (Brunskill et al., 2008). The selected RV-enriched genes were then compared to the expression profiles of control and *Wnt4* homozygous mutant kidneys (Valerius and McMahon, 2008). *Wnt4* mutant kidneys do not form nephrons but retain mesenchymal and ureteric epithelial structures. Genes were prioritized if they were RV-enriched and decreased in expression in *Wnt4* mutants and hence potentially critical for RV formation. A total of 63 genes showed statistically robust expression levels >4-fold higher in the renal vesicle compared to the other nephron structures and were added to 4 control genes previously reported to show expression in the RV (see Supplementary Table S1, available at http://grimmond.imb.uq.edu.au/gudmap/supplementaryData/index.html).

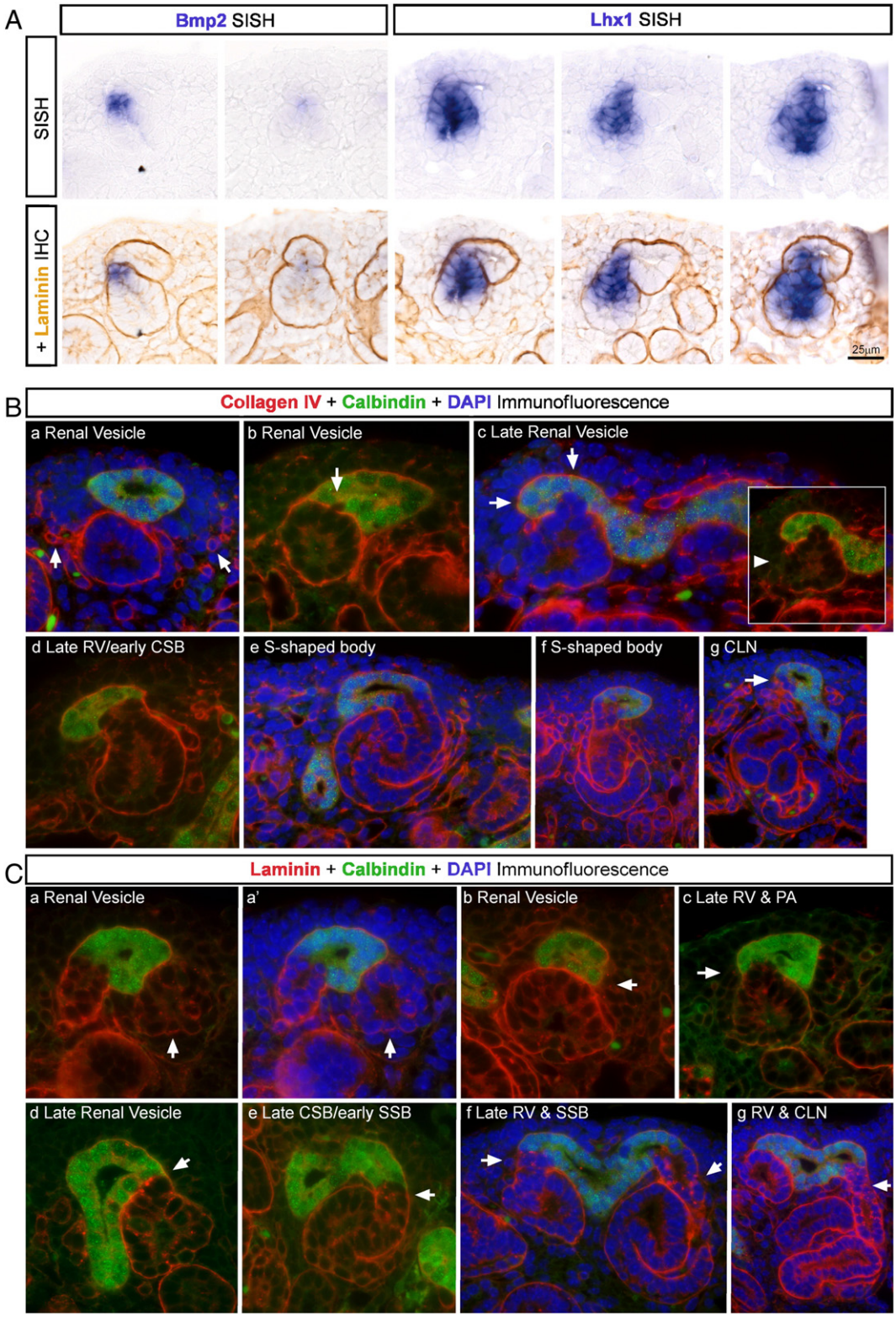

Polarization of gene expression in proximal and distal domains of the renal vesicle

Spatial expression of these genes at high resolution was examined using section *in situ* hybridization (SISH) of 15.5 dpc kidneys (Fig. 1). The annotated expression patterns, riboprobe details and SISH images for all genes analyzed are available on the GUDMAP website (www.gudmap.org). From this, it was possible to define expression in distal RV, proximal RV or complete RV. RVs showed polarized gene expression relative to the position of the ureteric tip and where the distal and proximal domains divided the RV in half (Fig. 1Bb). We also validated the reported distal RV expression of *Dll1* and *Pou3f3* (Kobayashi et al., 2005; Nakai et al., 2003) and proximal expression of the Wt1 protein (Georgas et al., 2008). The majority of polarized genes showed expression in the distal RV, as opposed to the proximal RV. To search for further polarized RV genes, we returned to the data of Brunskill et al. (2008) which contained four different RV samples and sought genes showing global expression patterns in the kidney that clustered with the two RV samples showing enriched distal RV expression versus the other two RV samples showing enriched expression of proximal markers (see Supplementary Fig. S1, http://grimmond.imb.uq.edu.au/gudmap/supplementaryData/index.html). A further 46 genes potentially polarized in the RV were identified, of which 32 were examined by SISH. The complete set of 112 renal vesicle genes validated by ISH is shown in Table S1. This is the largest set of genes examined in the renal vesicle of the developing kidney. Of the 112 genes, we identified 13 markers of distal RV and 2 markers of proximal RV (Fig. 1). Of the distal markers, 5 were enriched in the distal compared to proximal RV (*Ccnd1*, *Jag1*, *Ccdc86*, *Cdh6* and *Wnt4*), while the other 8 were specific to the distal RV (*Dkk1*, *Papss2*, *Greb1*, *Dll1*, *Pcsk9*, *Lhx1*, *Bmp2* and *Pou3f3*) and even demarcated subdomains of expression within the distal RV itself. *Tmem100* and *Wt1* were strongly expressed in the proximal RV (Fig. 1). Nephrons at later stages of development were also examined for expression of all genes. As anticipated, proximal RV markers continued to be restricted to the proximal segment in older nephrons (parietal (*Tmem100*) and visceral (*Wt1*) epithelia of the proximal S-shaped body (Stage II, Fig. 1C)). Similarly, distal RV markers were restricted to the medial and distal segments of the S-shaped body and later, to the tubular segments of Stage III–IV nephrons. Of significant note, distally restricted RV genes were not expressed in the developing renal corpuscle at any stage. Along the proximal–distal axis various overlapping molecular domains were observed within the tubules of these nephrons (Fig. 1C).

Increased cell proliferation in the distal region of the renal vesicle

Patterning of the nephron at such an early time point is likely to reflect differences in cell behaviour and prospective fate. Cyclin D1 (*Ccnd1*; G1/S-specific cyclin-D1), a marker of G1 phase of the cell cycle, displayed a polarized distal RV expression of the gene, which was mimicked by the expression of the protein (Figs. 1C, 2A). We therefore investigated whether the cells within the distal RV are proliferating more rapidly than cells within the proximal RV (Figs. 2B, C). Proliferating cells were semi-quantitatively analyzed in nephrons using expression of the mitosis marker phospho-Histone H3 (pHH3) (Hans and Dimitrov, 2001) detected via immunohistochemistry (IHC). *Wnt4* gene expression was used to identify pretubular aggregates and other early nephron structures in dual SISH/IHC (Georgas et al., 2008). Fig. 2Ba shows a typical pHH3 distribution in the 15.5 dpc kidney. The highest numbers of mitotic cells were detected in the nephrogenic zone. Comparable numbers of mitotic cells were identified in each of the early nephron stages (3.80% pretubular aggregate, 3.15% RV, 2.40% comma-shaped body and 3.90% S-shaped body). Statistically significant differences were observed in the number of mitotic cells detected in the distal versus proximal regions of the RV, with 73.5% of the mitotic cells present in the distal RV. The number of mitotic cells in the distal versus proximal S-shaped body and medial versus proximal S-shaped body was also significantly greater.

Lhx1 and Bmp2 may be involved in fusion of the renal vesicle with the ureteric tip

This SISH analysis of RV also revealed a set of genes (see Fig. 1) apparently additionally expressed in a region of the adjacent ureteric tip (UT) in the location where these two adjacent compartments must fuse. Two genes expressed in this early connecting segment were *Lhx1* and *Bmp2*. We have previously shown that the connecting segment of the RV, whilst appearing to lie within the UT epithelium, does not express the UT marker Calbindin (*Calb1*; Calbindin D28K) (Georgas et al., 2008), suggesting that this segment may arise from the RV rather than the UT. In order to investigate this further, we examined the basement membrane (BM) of both these epithelial structures using dual SISH/IHC. Fig. 3A shows that the domains of *Lhx1* and *Bmp2* expression observed pushing up into the UT were not crossed by collagen IV and laminin. A further detailed spatial and temporal analysis (across each stage of nephron formation) using immunofluorescence with antibodies to Calbindin to mark the ureteric epithelium and collagen IV or laminin to mark the BM also suggested the loss of BM between the renal vesicle and the UT at what appeared to be the RV stage (Figs. 3B, C). However small, punctuate spots of laminin expression were occasionally seen within the connecting segment, not only of RV stage nephrons (Figs. 3A, Cc, d), but also in the more mature connecting tubule of nephrons at older stages; Stages II–III (SSB and CLN, Fig. 3Ce–g) and maturing Stage IV nephrons (data not shown).

Fig. 3. Analysis of the basement membrane during early nephron formation. The basement membranes (BM) of the ureteric epithelium and early nephrons were examined in sagittal sections of 15.5 dpc kidneys using antibodies to the BM markers, collagen IV and laminin. (A) SISH images of RVs showing expression of the distal RV genes *Bmp2* and *Lhx1* in the connecting segment of the RV (top panel). IHC using anti-laminin (orange) antibody to mark BM was performed after SISH on the same tissue (bottom panel). The domains of *Bmp2* and *Lhx1* expression were not crossed by the laminin + BM or the collagen IV + BM (images not shown). (B–C) The BM was examined in nephrons at various stages by immunofluorescence using antibodies to collagen IV and laminin (red). The ureteric tip (UT) was visualized with anti-Calbindin antibody (green) and DAPI was used to visualize cell nuclei (blue). (B) Collagen IV: (a) Section through an RV shows the RV surrounded by its own BM and separated from the adjacent UT by the ureteric epithelial BM. Cells adjacent to the cap mesenchyme which express collagen IV are likely to be developing endothelial cells (arrows). (b) Section of an RV shows a single cell (Calbindin −ve) extending into the UT and here a gap is seen in the BM (arrow). The remainder of the RV is surrounded by BM. (c) Section of an RV clearly shows three cells (Calbindin −ve) extending into the UT and not separated from the tip by BM (arrow). Note that this RV does not display a complete BM, there is no BM on the side adjacent to the cap mesenchyme (arrowhead in inset). (d–g) Later in nephrogenesis the nephron connection to the UT is complete and they share a continuous BM and lumen. Examples are shown for (d) late RV/early CSB, (e) early SSB, (f) late SSB and (g) CLN. C. Laminin: (a) The cells of an early RV (arrow) show weak laminin expression. (a′) The presence of a central lumen indicates that this is an RV and DAPI staining shows the organization of the nuclei. (b) Section through an RV surrounded by BM and separated from the adjacent UT by BM. (c) Section of a late RV shows a group of cells (Calbindin −ve) extending into the UT (arrow). The remainder of the RV is surrounded by BM. Cells of a PA on the right of the tip show some evidence of weak laminin expression. (d) Section through a late RV surrounded by BM which is continuous with the BM of the UT. At the junction between the RV and the UT (arrow) a gap can be seen in the BM between the tip cell (Calb +ve) and the adjacent RV cell (Calb −ve). Spots of laminin are observed at the connection point between the two different cells. (e–g) Later in nephrogenesis the nephron connection to the UT is complete and they share a continuous BM and lumen. As seen in the RV in d, spots of laminin were often seen in the connecting region (arrows in d–g). Examples are shown for (e) late comma/early SSB, (f) late RV and SSB and (g) CLN. BM = basement membrane, UT = ureteric tip, PA = pretubular aggregate, RV = renal vesicle, CSB = comma-shaped body, SSB = S-shaped body, CLN = capillary loop nephron.

Morphological changes in the renal vesicle simultaneous with fusion with the ureteric tip

The difficulty with these approaches is the definitive identification of a renal vesicle from a slightly later comma- or S-shaped body, which will also appear as a roughly spherical object depending upon the plane of section. To further analyze the process of RV fusion with the UT in 3-dimensions, confocal microscopy was performed on wholemount 15.5 dpc kidneys stained for Calbindin (to label the UT) and collagen IV (basement membrane, BM) by immunofluorescence (Fig. 4). This enabled 3D reconstruction of the nephrogenic zone of the kidney from optical sections collected to a depth of 34 to 58 μm deep (approximately 30 slices taken every 1–2 μm). Viewed from the capsular surface of the kidney this revealed the appearance of cavitations within the Calbindin staining on the underside of the ureteric tips which are not separated from the early nephrons by a BM. This again suggests that fusion has occurred via the insertion of RV-derived cells into the ureteric tip. Movies animating the examples shown in Fig. 4 can be viewed as Supplementary movies 1 and 2 (available at http://grimmond.imb.uq.edu.au/gudmap/supplementaryData/index.html).

To more precisely stage the early nephron structures to confirm the timing of fusion, 3D models were also created using immunofluorescence of 15.5 dpc kidney serial sections labeled with Calbindin (UT) and collagen IV (BM). This approach enabled the visualization of multiple nephron stages and revealed their relationship to the ureteric tree in 3D (Fig. 5). Supplementary movies 3–5 (http://grimmond.imb.uq.edu.au/gudmap/supplementaryData/index.html) show the results of this modeling, which revealed the very complex nature of nephrogenesis within the nephrogenic zone. Models showed that the terminal UB generally has two to three tips from a common ampulla, that early nephrons around a common terminal UB are rarely at the same stage of maturation as each other and that any given tip has

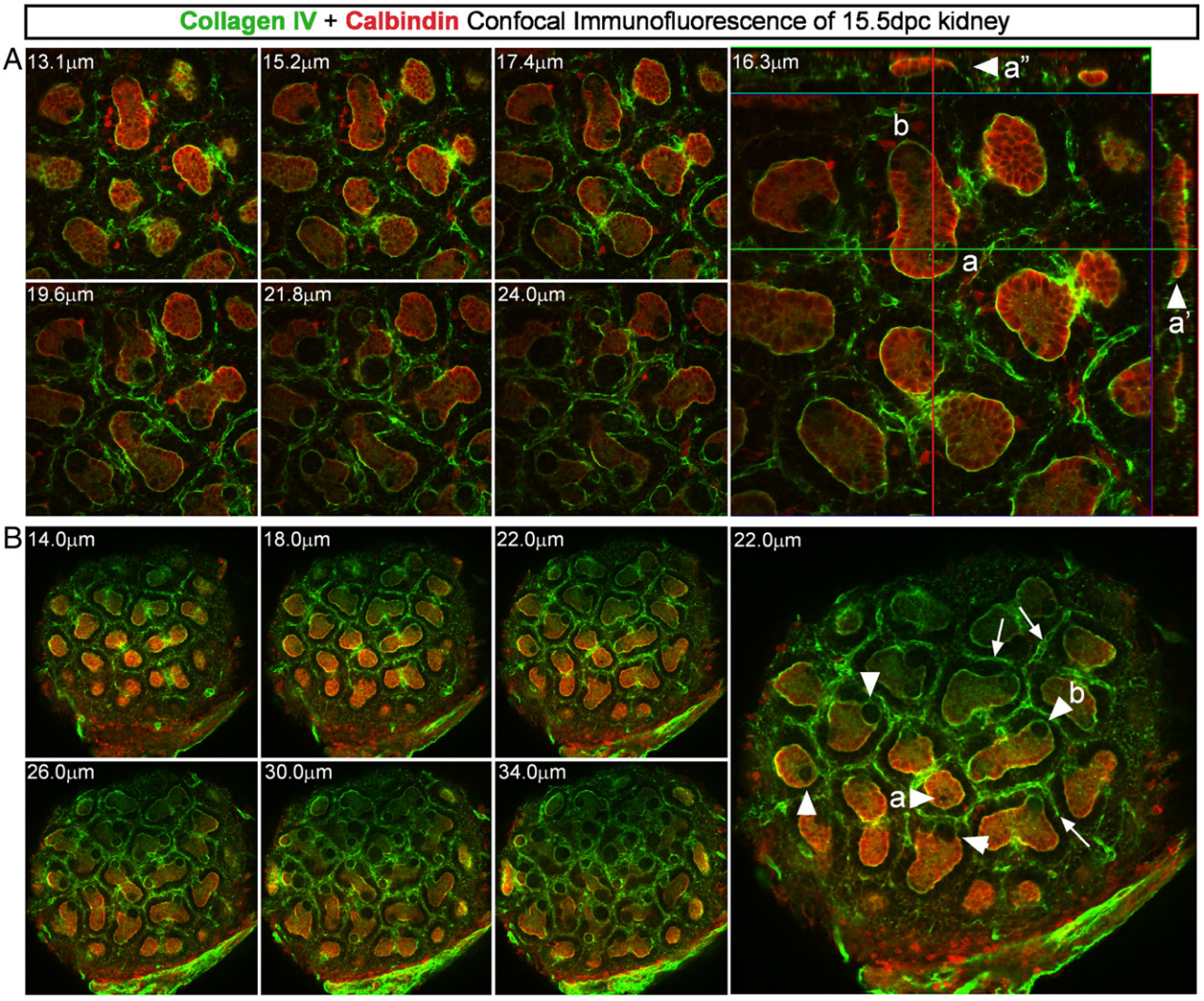

Fig. 4. Confocal immunofluorescence of nephrons and their connection to the ureteric tips. Panels A and B are two examples of immunofluorescence on wholemount 15.5 dpc kidneys. Optical serial sections were taken through the nephrogenic zone and outer cortex using confocal microscopy. The basement membrane (BM) was labeled with anti-collagen IV antibody (green) and ureteric tips (UT) with anti-Calbindin antibody (red). (A) A 325.75 μm × 325.75 μm region scanned as a stack 33.77 μm deep comprised of 30 slices taken every 1.09 μm looking down on the nephrogenic zone from the outside of the kidney (40×/0.75). A subset of 6 slices is shown on the left. The enlarged image on the right shows an orthogonal section view at 16.3 μm mid-way through the stack. A nephron (a) is connected to the UT via a small group of cells which do not express Calbindin but are surrounded by BM (a). In the side views (sagittal (a′) and transverse (a″) sections through the UT) arrowheads indicate the position of these Calbindin −ve cells extending into the UT from the nephron. The nephron at the other end of the same UT (b) is more mature and has a BM continuous with the tip (b). (B) A 651.5 μm × 651.5 μm region scanned as a stack 57.98 μm deep comprised of 32 slices taken every 2.0 μm looking down on the nephrogenic zone from the outside of the kidney (20×/0.75). A subset of 6 slices is shown on the left. The enlarged image on the right shows a cut through the stack at 22.0 μm. Each UT has a nephron connected to it via a connecting segment which does not express Calbindin (arrowheads). Some Calbindin −ve connecting segments are not surrounded by BM (a) and some have a BM contiguous with the tip (b). Note that a collagen +ve BM can be seen surrounding each UT on the outer edge of the cap mesenchyme (arrows). It is possible that these cells are developing endothelial cells lying adjacent to the cap mesenchyme. Movies animating these two examples can be viewed as Supplementary movies 1(A) and 2(B) (available at http://grimmond.imb.uq.edu.au/gudmap/supplementaryData/index.html).

more than one nephron attached to it at any one time. 3D modeling also enabled the definitive categorization of nephrons into RV, comma-shaped, S-shaped and Stage III capillary loop nephron stages (Fig. 5), revealing that early RVs were not fused to the UT and were roughly spherical in shape (Fig. 5C). In contrast, late RVs were connected with the UT and had started to widen at the proximal end (Figs. 5A, B). In addition to changes in morphology, early RVs displayed only a partial covering of BM (based on collagen IV expression) with gaps detectable in the BM especially noticeable on the side of the RV adjacent to the cap mesenchyme. We did not find any evidence to suggest that the distal renal vesicle cells closest to the ureteric tip form their own basement membrane. However, early RVs were separated from the adjacent ureteric tip by the BM of the tip epithelium (Fig. 5Cb–d′). Late 'connected' RVs had between 1 and 5 cells pushed up into the UT and there was no longer a basement membrane separating the two structures (Figs. 5A, B). Hence, late RVs are an intermediate stage between RV and comma-shaped body as they lack two hallmarks of the comma-shaped body stage, a cleft and elongation of the proximal cells. In contrast, these structures have a general broadening of their proximal end with only a small group of cells within this region beginning to protrude out from the main body of the RV (Figs. 5A, B).

Origin of the cells of the connecting tubule

In order to definitively determine the origin of the cells of the connecting tubule, we used the *Six2-TGC eGFP Cre*-driver strain (Kobayashi et al., 2008a) crossed to *R26R-lacZ* reporter mice to label nephron cells derived from the cap mesenchyme. Kidney sections were analyzed at 15.5 dpc and examples of the images obtained are shown in Fig. 6A. The *Six2-TGC* expressing cells are shown in green (eGFP), while all derivatives of these cells are labeled by βgal expression shown in red. The collecting duct is visualized with Cytokeratin (violet). This shows that fusion is completed at the late RV stage, in agreement with all other data presented here. The connecting segment of the nephron, first visible at the late RV stage, is derived from the *Six2*+ cap mesenchyme. It should also be noted that the expression of *Six2* appears to persist in the proximal RV. This may represent continued and polarized gene expression of *Six2* in the RV or a delay in degradation of the reporter. Hence, either the proximal end of the RV is the last part to become incorporated into the aggregate or that signals from the UT more rapidly depress *Six2* expression in the adjacent distal RV compared to the proximal portion of the RV.

Expression of E-cadherin in the RV occurs after fusion to the ureteric tip

The transition from pretubular aggregate to RV is commonly referred to as a mesenchymal to epithelial transition event, implying that the resulting RV is epithelial. E-cadherin (*Cdh1*) is critical for the formation of cell–cell contacts in epithelia irrespective of their origin from ecto-, meso- or endodermal tissue and is widely used as an indicator of a mature epithelium. Hence we sought to further characterize its expression during nephron formation using immunofluorescence (Fig. 7). Not surprisingly, Stage III and IV nephrons show strong levels of E-cadherin expression on the cell membrane of early proximal, distal, loop of Henle (immature and anlage) and renal connecting tubules. E-cadherin protein was also seen in the renal connecting segment and distal and medial segments of the S-shaped body stage. Expression was absent from the proximal segment as shown previously (Cho et al., 1998; Dahl et al., 2002). Interestingly, only moderate expression was seen in the distal or upper limb of the comma-shaped body, even after the nephron connects with the UT. Expression was undetectable in the early and late RV (Figs. 7a, b). Hence, E-cadherin protein is not detectable on the cell membrane until after the nephron has completely fused with the UT, between the late RV and comma-shaped body stages.

The previously reported polarized expression of the cadherins, including Cadherin-6 and E-cadherin in the proximal and distal RV respectively (Cho et al., 1998), was not supported by our data. We found strong *Cdh6* expression in the distal RV and only weak expression in the proximal RV. However, as seen in later nephron stages, the restricted gene expression of *Cdh6* in the medial S-shaped body (see Fig. 1) and expression of the E-cadherin protein in the medial and distal S-shaped body (see Fig. 7) are in concordance with the reported proximal–distal cadherin patterning such that proximal tubule precursors express Cadherin-6 and more distal tubule precursors express E-cadherin (Cho et al., 1998). It is possible that the previous interpretation of cadherin patterning in the RV was based on observations of a later stage of nephron development than presumed.

Discussion

Fusion between two epithelial surfaces is a common and crucial process in the normal development of a number of tissues. Such fusion events occur in palatal shelf fusion, neural tube closure and branchial arch remodeling to form the face (Nawshad, 2008). In all these events, the two epithelial surfaces meet at their apical surfaces, lamellipodial processes protrude from the apical surfaces and the epithelial cells change shape to create new cell–cell contacts. This surface ruffling is similar to the processes observed in wound healing and involves the Rac/Rho pathways and microfilament rearrangement (Jacinto et al., 2001). The completion of palatal fusion to form a single new epithelial layer is also thought to involve apoptosis and an epithelial to mesenchymal transition to complete the removal of the palatal seam (Nawshad, 2008). In contrast, fusion of the renal vesicle (RV) with the ureteric tip (UT) requires fusion between two basal surfaces. Nothing is understood about such fusion events.

The distal RV abuts the UT and represents the pole of the RV which will fuse with the ureteric epithelium. In this study, we have identified a number of genes which are upregulated or specifically marker the distal RV. We have also demonstrated that the process of fusion between these two structures required the restructuring of the basement membrane and occurs at the late RV stage via a fusion in which cells of the distal RV impinge onto the ureteric tip, potentially driven by preferential cell division within the distal RV. We have also shown that E-cadherin expression and a mature epithelial phenotype do not exist until after this fusion event has occurred.

Disruption to genes expressed within the RV is known to result in failure to form either the entire nephron (*Lhx1*, *Wnt4*) or certain segments of the nephron (*Pou3f3*, *Jag1*, *Notch2*). For example, in *Wnt4* knockout mice, the formation of nephrons is blocked at the pretubular aggregate stage (Kispert et al., 1998; Stark et al., 1994). The distal RV gene *Pou3f3* (*Brn1*) is required for the differentiation of the distal nephron (loop of Henle and distal convoluted tubules) (Nakai et al., 2003) and *Notch2* and *Jag1* for proximal nephron structures, including the glomerulus and proximal tubules (Cheng et al., 2007; Cheng and Kopan, 2005; McCright et al., 2001; McCright et al., 2002). Loss of nephron segmentation appears to correlate with genes that show polarized expression in the RV. Inactivation of *Lhx1* in the metanephric mesenchyme (Rarb2-Cre transgene) results in the formation of RVs that express *Wnt4*, but fail to show polarized expression of *Pou3f3* and *Dll1* (Kobayashi et al., 2005). This failure to polarize the RV arrests nephron development at this stage, resulting in small, non-functional kidneys without nephrons. In chimera experiments using *Lhx1*$^{-/-}$ embryonic stem cells these *Lhx1* null cells were excluded from the distal nephron and could only contribute to the parietal and visceral epithelia of the proximal S-shaped body (Kobayashi et al., 2005), consistent with a role for *Lhx1* in specification of the distal nephron.

This study has confirmed the polarized expression of a number of known genes, but has also greatly expanded the number of genes showing polarized RV expression patterns. We would predict that

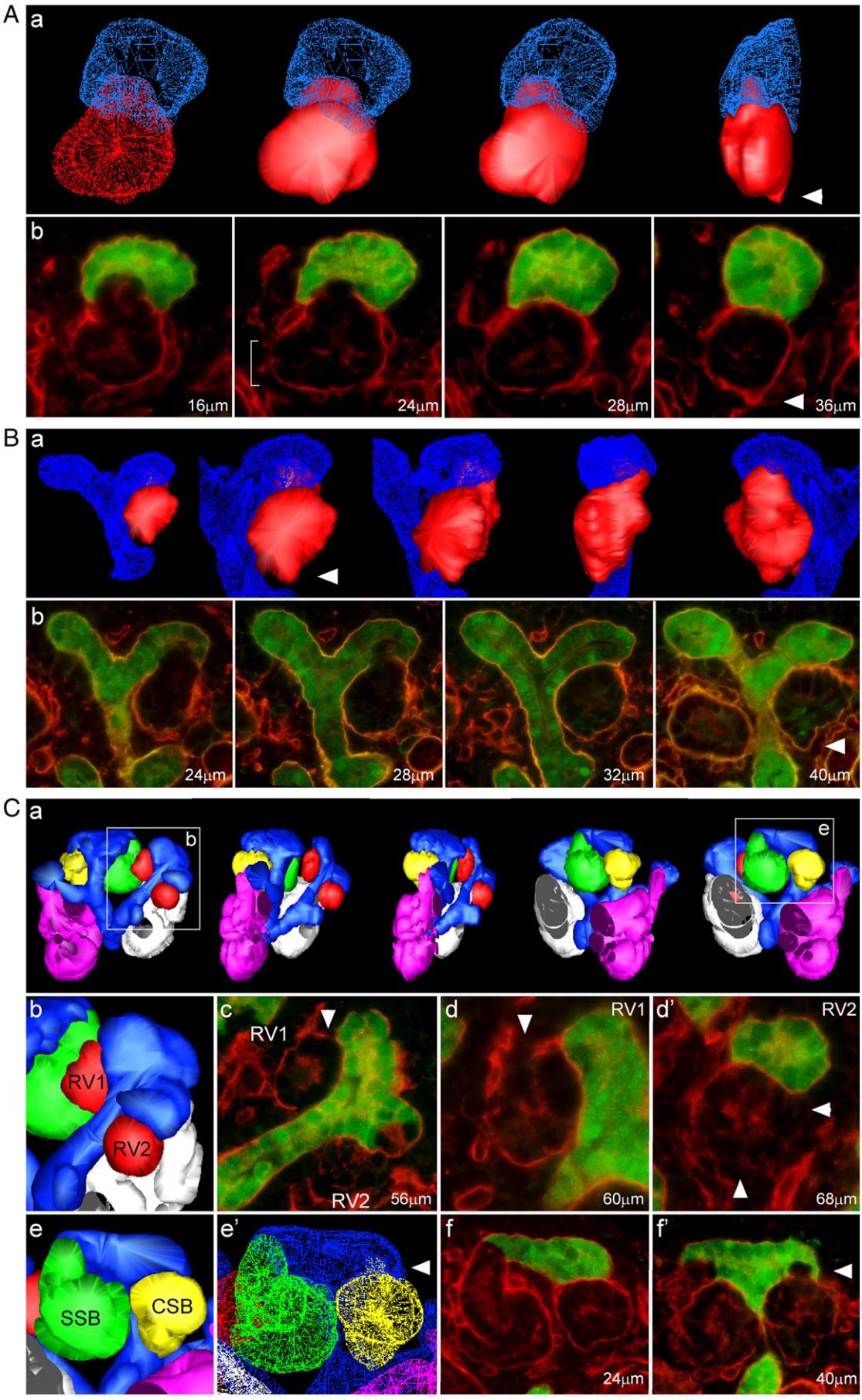
A
a
b
16μm
24μm
28μm
36μm
B
a
b
24μm
28μm
32μm
40μm
C
a
b
e
b
RV1
RV2
c
RV1
RV2
56μm
d
RV1
60μm
d'
RV2
68μm
e
SSB
CSB
e'
f
24μm
f'
40μm

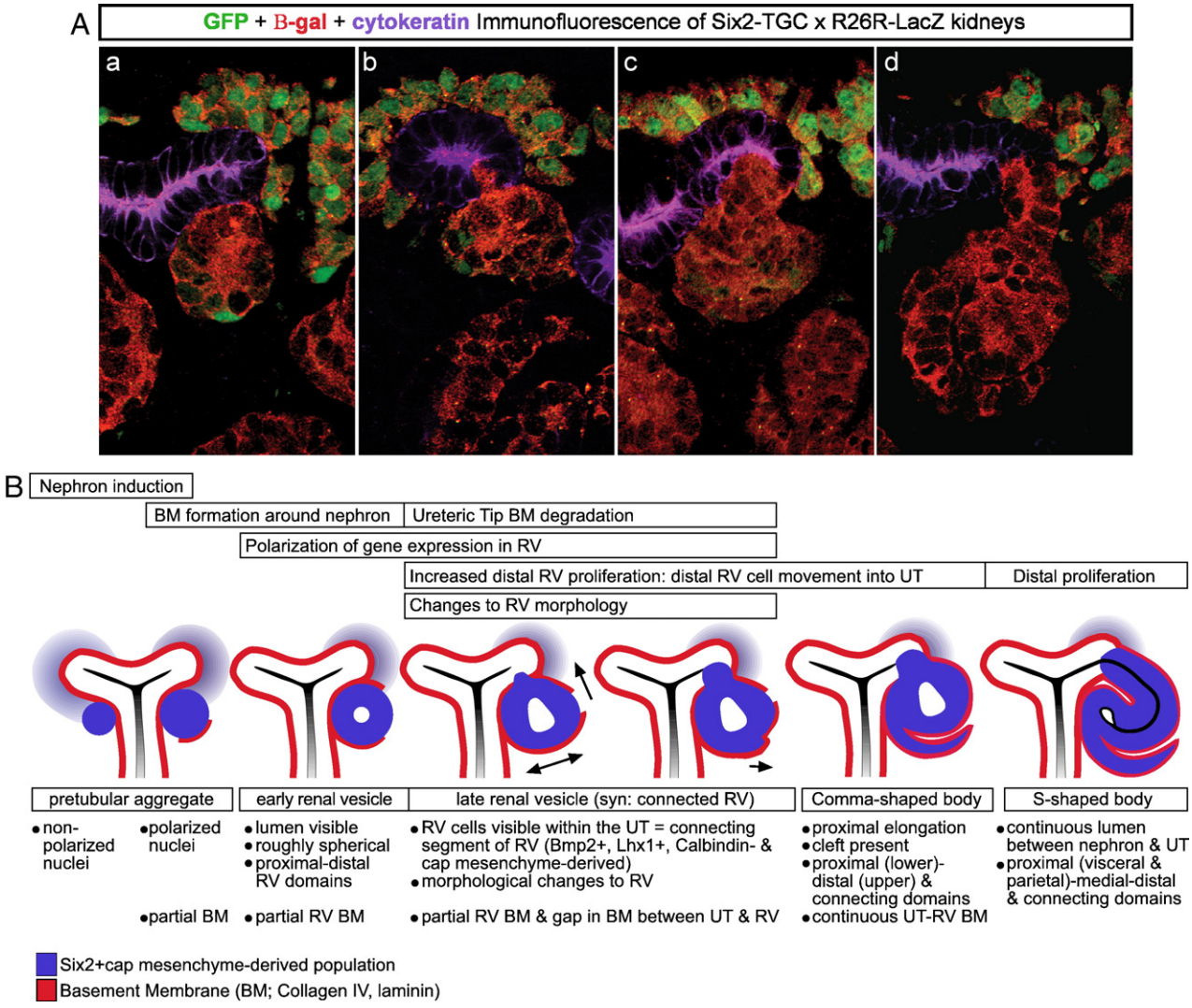

Fig. 6. The cellular origin of the connecting segment and a model of the fusion event. A. Kidneys from *Six2-TGC/R26R-lacZ* mouse strain were analyzed to determine the origin of cells in the connecting segment. Confocal immunofluorescence shows the *Six2*-expressing cap mesenchyme (GFP — green), cap mesenchyme-derived cells (βgal — red) and ureteric tips (UT, labeled with anti-cytokeratin antibody — violet). (a) Renal vesicle (RV) juxtaposed tightly with the UT. (b) A more mature RV showing the initial stages of the connection event. βgal+ (red) cap mesenchyme-derived cells insert into the UT (violet). (c) An early nephron (late RV / early comma-shaped body) with a well established connection to the UT. The connecting segment is βgal+. (d) A mature S-shaped body (note the extension of the connecting segment with a well defined boundary at the junction to the UT). B. A model describing the process and timing of the fusion between the late renal vesicle and the ureteric tip. The growing ureteric epithelium is surrounded by a basement membrane (BM). BM of all renal structures is shown in red. The nephron develops from the Six2+ population of cap mesenchyme (shown in blue) and through a series of stages undergoes MET from mesenchymal pretubular aggregate (left) to the epithelial S-shaped body (right). Proximal–distal patterning of the nephron is simultaneous with its epithelialization and fusion.

defects in these genes are also likely to affect patterning and/or fusion of the RV to the UT. Pathway analysis suggests the involvement of the notch (*Jag1*, *Dll1*), BMP (*Bmp2*) and Wnt (*Wnt4*, *Dkk1*, *Ccnd1*) signaling pathways in distal RV patterning (see Supplementary Fig. S2 available at http://grimmond.imb.uq.edu.au/gudmap/supplementaryData/index.html). Wnt signaling can activate the canonical β-catenin pathway or the non-canonical planar cell polarity pathway (PCP) (also activated by notch), which recruits small GTPases of the rho/

Fig. 5. 3D modeling reveals the morphological structure of the developing renal vesicle. 3D models of nephrons connected to the ureteric tree were created from serial section immunofluorescence of 15.5 dpc kidneys using anti-collagen IV antibody to visualize the basement membrane (red) and anti-Calbindin antibody (green) to visualize the ureteric tree. IF images were reconstructed using a 3D modeling program whereby each structure (nephron and ureteric tree) was outlined and rendered into a 3D model. Lateral views of the models are shown either in wire view (outline) or filled view. Movies of the 3D models are available as supplementary data (Supplementary movie 3(A), movie 4(B) and movie 5(C) at http://grimmond.imb.uq.edu.au/gudmap/supplementaryData/index.html). A. A single late renal vesicle (RV) connected to the adjacent ureteric tip (UT). (a) 3D model shown rotating 90° shows the RV in red and UT in blue. (b) Representative IF images show the RV connected to the UT, the connecting region is not separated by BM (red) (see 16 and 24 μm) and sections through the outer edge of the RV show BM between the RV and the UT (28 and 36 μm). B. A terminal branch of the ureteric tree and associated nephrons. (a) 3D model of this region (only one nephron, the RV on the right has been modeled) shown rotating 90° shows the RV (red) connected to the adjacent UT (blue). (b) Representative IF images show the RV connected to the UT, the connecting region is not separated by BM (red) (see 26 and 26 μm) and sections through the outer edge of the RV show BM between the RV and the UT (32, 40 μm). *Note:* the RVs in A and B are late RVs; they are fused to the UT and their proximal pole shows changes in morphology including widening (indicated in Ab, 24 μm) and small region protruding out from the main body of the RV (arrowheads in A and B). C. A region of the outer edge of the kidney including three terminal branches of the ureteric tree. (a) 3D model of this region shows the ureteric tree (blue) and associated nephrons including; 2 RV (red), CSB (yellow), SSB (green) and 2 CLN (pink and white). (b–d′) Enlargement of one terminal tree branch containing 2 early RVs. (c–d′) Representative IF images show RV1 and RV2 are not connected to the UT and are roughly spherical in shape. Both RVs show an incomplete BM, most notable on the side adjacent to the cap mesenchyme and farthest from the ureteric tree (arrowheads in c–d′). (e–f′) Enlargement of region within the model containing SSB and early CSB is shown. (e′) Wire model shows the small connecting tubule region of this early CSB pushing up into the UT (arrowhead). (f, f′) Representative IF images show SSB and CSB both connected to the UT. SSB shows a broad connection region the same width as the UT (f) and CSB shows only small region pushing up into the UT (arrowhead in f′). RV = renal vesicle, CSB = comma-shaped body, SSB = S-shaped body, CLN = capillary loop nephron.

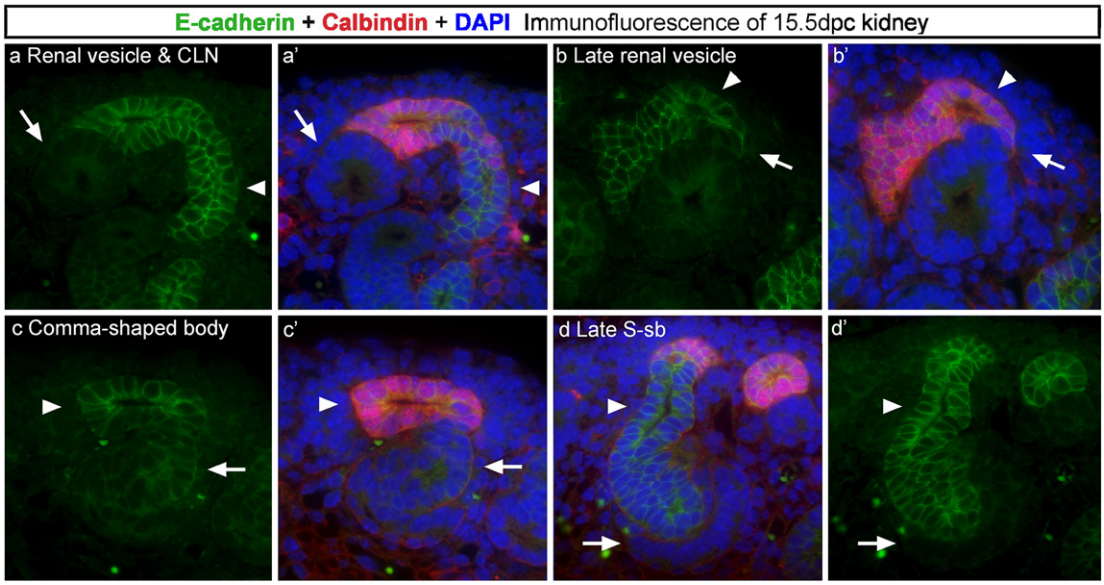

Fig. 7. Analysis of E-cadherin expression during early nephron formation. IF was used to examine the protein expression of E-cadherin (green) in renal vesicles (RV) and early nephrons and is indicative of a mature epithelium. The ureteric tip was visualized with anti-Calbindin antibody (red) and DAPI was used to visualize cell nuclei (blue). Images are shown with (′) and without DAPI staining. (a) At the RV stage, the nephron does not express E-cadherin on the cell membrane (arrow). The RV does display characteristics of an epithelial structure; the presence of a central lumen and the polarized organization of the nuclei. The more mature nephron on the right (capillary loop stage) connected to the ureteric tip shows strong expression in its renal connecting tubule. (b) A late RV shown with a small group of cells (Calbindin −ve) extending into the ureteric tip (arrow). This late RV including the connecting segment does not express E-cadherin on the cell membrane. (In a and b, the weak diffuse fluorescence surrounding the RV lumen was considered to be non-specific background.) Strong E-cadherin/Calbindin co-expression is seen in the ureteric tip (arrowhead). (c) At the comma-shaped body stage the connection of the nephron to the ureteric tip is complete. Moderate expression can be seen in the distal CB (arrow). Strong E-cadherin/Calbindin co-expression is seen in the ureteric tip (arrowhead). (d) By the S-shaped body (SB) stage strong E-cadherin expression can be seen in all the tubular components of the nephron (including renal connecting tubule and distal and medial SB segments) (arrowhead). Expression is absent from the proximal segment of the SB which will become the renal corpuscle.

cdc42 family to activate JNK (Dressler, 2008). Rho/cdc42 activity is also involved in wound healing and classical fusion in other tissues. It is canonical Wnt signaling that has been described as being required for nephron initiation as knockouts of *Wnt4* fail to form renal vesicles (loss of MET) (Stark et al., 1994). The dickkopfs, including the distal RV gene *Dkk1*, inhibit canonical Wnt signaling by binding to Lrp5/6 co-receptors, forming a ternary complex with frizzled receptors (Niehrs, 2006). However, *Dkk1* can also induce apoptosis and activate JNK, suggesting crosstalk with the PCP pathway. As well as the distal RV, *Dkk1* was also expressed in the surrounding interstitium immediately next to the RV. This may indicate a feedback loop inhibiting the adjacent ureteric epithelial *Wnt9b* signal to allow fusion to occur. While *Wnt4* and *Wnt9b* are known to be crucial for MET in the kidney, a recent study using TCF/Lef-LacZ reporter mice has shown that canonical Wnt signaling is active not only in the ureteric tree, but also in developing nephrons at the S-shaped body stage (Schmidt-Ott et al., 2007). This is consistent with a role for canonical Wnt signaling in nephrogenesis and was correlated with the expression domains of *Emx2*, *Pax8* and *Ccnd1* which were identified as putative TCF/Lef target genes. Two of these genes, *Pax8* and *Ccnd1*, we have shown to be strongly expressed in the RV, with *Ccnd1* strongly upregulated in the distal RV. *Pax8* is a transcription factor which acts cooperatively with *Pax2* to regulate cell survival and lineage specification of the early metanephric mesenchyme and later, the differentiation of distal nephron segments (Bouchard et al., 2002; Narlis et al., 2007). *Ccnd1* has been verified as a β-catenin-induced TCF/Lef target gene in colon carcinoma cells (Tetsu and McCormick, 1999). In this study we speculate that CyclinD1 (*Ccnd1*) has the potential to be a critical player in early nephron development by regulating proliferation in the distal nephron which may subsequently drive the fusion of the nephron with the ureteric tip. These events may be activated via the canonical Wnt signaling pathway.

Notch signaling is involved in lateral inhibition, lineage decision making and boundary/niche formation. It has previously been shown that the Notch pathway is critical for proximal tubular development and shows polarized activity at the S-shaped body stage of nephron development and earlier (Dressler, 2008; Leimeister et al., 2003). *Notch2* and its ligand *Jag1*, are critical for proximal tubule and glomerular development (Cheng et al., 2007; McCright et al., 2001; McCright et al., 2002). Disruption of *Notch2* results in a loss of Cadherin-6 expression in the kidney (Cheng et al., 2007), hence undoubtedly disrupting RV patterning. We found *Cdh6* expression upregulated in the distal RV and mutation of this gene results in nephrons which fail to fuse to the ureteric tip which is thought to be the result of a delay in MET (Mah et al., 2000). Of interest, it has also been shown that several Notch pathway members re-express in the proximal tubules in response to ischaemic damage (Kobayashi et al., 2008b) and the TGFβ-induced induction of an EMT involves *Jag1* and its target *Hey1* (Zavadil et al., 2004). Hence, the distal RV may either represent a region of the nephron where there is a reversion of MET or a delay in proper epithelialization. This may be critical for the process of fusion of the RV with the adjacent UT. Contrary to this thinking is the apparent persistence of *Six2* in the proximal RV suggesting that this region is the last to undergo MET. Additional evidence to support this comes from the expression pattern of the epithelial cadherin, *Cdh6* which was strongly upregulated in the distal RV and is consistent with the concept that the proximal RV is the last region to epithelialize.

Bmp2 expression has previously been implicated in the regulation of ureteric epithelial proliferation (Hartwig et al., 2005). Distal *Bmp2* signaling may regulate UT branching and mitosis, again to facilitate fusion between the RV and the UT. Using a BMP signaling reporter mouse, it has been shown that SMAD signaling in the kidney is present in the ureteric compartment, but not the tips (Blank et al., 2008). Upon closer inspection signaling is biased to the side of the UT adjacent to the *Bmp2*-expressing RV connecting segment.

In addition to these well characterized genes, several poorly understood genes were also expressed in distal RV. These included *Papss2*, *Pcsk1* and *Greb1*. *Papss2* produces a bifunctional enzyme responsible for sulfation of proteins, carbohydrates, and lipids.

Sulfation of extracellular matrix proteins, such as the proteoglycans, modulates cell adhesion. Sulphated proteoglycans are known to be critical during early kidney development. Chlorate inhibition of sulphated GAGs during kidney explant culture disrupts ureteric branching (Davies et al., 1995) while Heparan sulfate 2-O-sulfotransferase 1 (*Hs2st1*) knockout mice show perinatal lethality due to renal agenesis (Wilson et al., 2002). *Papss2* is mutated in murine Brachymorphism (*Papss2*^{bm}), an autosomal recessive disease which primarily affects the skeleton due to reduced sulfation of proteoglycans (Kurima et al., 1998). Other tissues that contain important sulfated biomolecules, including the kidney and brain, appear normal in *Papss2*^{bm} mice, however the protein activity was shown to be only moderately affected in these mice (Sugahara and Schwartz, 1982). Of note, the activity of Bmp2 has been reported to be affected by sulfation of proteoglycans (Osses et al., 2006), an activity potentially regulated by Papss2.

Proprotein convertase subtilisin/kexin type 9 (*Pcsk9*) is described as a plasma protein involved in lipid metabolism via the degradation of low density lipoprotein receptor (LDLR). However, it is a proprotein convertase related to PACE, furin and other enzymes involved in the proteolytic processing of TGFβ and BMPs, which are synthesized as proproteins requiring cleavage for activation. Of note, disruption of *Pcsk9* in the liver disrupts liver regeneration (Zaid et al., 2008); hence expression of this gene in the distal RV may play a role in cell turnover. Gene regulated by estrogen in breast cancer protein (*Greb1*) is an estrogen-receptor target gene induced by estradiol in breast cancer cells. Nothing is known about the function of this gene.

Using 3D modeling of fluorescently labeled RV and UT structures within the kidney, we have been able to examine in detail the process of RV fusion to the UT and propose here a model in which fusion occurs at the late RV stage (see Fig. 6B). In this model, proximal–distal patterning of the early nephron occurs simultaneously with its conversion from mesenchymal aggregate to epithelial nephron and fusion to the UT. The initial MET from pretubular aggregate to RV involves cell polarization. Both aggregates and RVs express proteins involved in this process such as the cadherin, *Cdh4* (R-cadherin) and the tight junction protein, ZO-1 (K. Georgas and M.H. Little unpublished observations; Mah et al., 2000) which promotes and maintains epithelial cell polarization via cell–cell adhesion. By the early RV stage these polarized vesicles have developed a central lumen and they express *Cdh6* (Cadherin-6). However, the RV displays an immature epithelial phenotype due to the absence of E-cadherin. During MET a partially formed basement membrane is produced around the RV and is marked by the expression of laminin and collagen IV. It is possible to see RVs which are completely separated from the ureteric epithelium by basement membrane. It is only once there is an initial change in morphology of the RV, potentially driven by differential gene expression resulting in RV elongation and a change in lumen shape, that there is a reduction in the ureteric epithelial basement membrane between the distal RV and the adjacent UT. As a result, initially a single cell appears within the UT that no longer expresses UT markers. Lineage tracing has confirmed that such cells are derived from the RV and does not result from a fate change within the ureteric epithelium. The presence of RV-derived cells in this location may result from changes to the plane of division within the RV, potentially due to activity of the PCP pathway, and/or cell migration or adhesion resulting in what appears to be an invasion of the tip. The ureteric epithelial basement membrane between the RV and ureteric tip is lost as the distal RV region expands into the UT. This is clearly accompanied by an increased rate of distal RV proliferation. A continuous basement membrane and a completely patent lumen linking the early nephron with the ureteric epithelium are evident by late comma/early S-shaped body stage, at which time E-cadherin is expressed in the distal renal epithelium of the fused nephron.

This study represents the most thorough investigation to date of early nephron formation. Here, we have carefully documented the process of early nephron patterning and fusion via high resolution analyses of gene expression and RV morphogenesis across the process of nephron development. This study adds eleven genes to the three previously known to be regionally expressed in the RV and implicates them in nephron patterning and/or fusion. Careful dual ISH/IHC and IF analyses in normal and transgenic (*Six2*-labeled) kidneys across time have also revealed that fusion occurs at a late RV stage, prior to E-cadherin expression, and that the connecting segment is a derivative of the cap mesenchyme. Future analyses of the role of these genes using specific targeting of the RV subcompartments coupled with live imaging and lineage tracing will enormously improve our capacity to dissect nephron patterning throughout the entire course of nephron formation. The implications of disruption to early events in nephron patterning and fusion include reduced or non-patent nephrons. A greater understanding of the fusion process may also have wider implications for our understanding of the molecular basis of this type of fusion event in this and other organs and how closely it resembles other forms of fusion and wound repair.

Acknowledgments

We wish to thank Jane Brennan, Jane Armstrong, Sue Lloyd-McGilp, Chris Armit and Jamie A. Davies (Edinburgh University, Scotland) and Derek Houghton, Ying Cheng, Xingjun Pi, Mehran Sharghi, Simon Harding and Duncan R. Davidson (MRC Human Genetics Unit, Western General Hospital, Scotland) within the Editorial and Database Development Offices of GUDMAP respectively for their support and assistance in annotating and uploading data to the GUDMAP database http://www.gudmap.org, which is supported by the NIH-NIDDK. Confocal microscopy was performed at the ACRF/IMB Dynamic Imaging Centre for Cancer Biology, established with the support of the Australian Cancer Research Foundation. The work presented in this manuscript was supported by the National Institutes of Health-NIDDK research grants to M.H.L and S.G — DK070136, S.S.P — DK070251 and A.P.M — R37 DK054364. M.T.V. was supported by a National Research Service Award (NRSA) (NIH-NIDDK F32DK060319). S.G and M.H.L are Research Fellows of the National Health and Medical Research Council of Australia.

Appendix A. Supplementary data

Supplementary data associated with this article can be found, in the online version, at doi:10.1016/j.ydbio.2009.05.578.

References

Bard, J.B.L., Gordon, A., Sharp, L., Sellers, W.I., 2001. Early nephron formation in the developing mouse kidney. J. Anat. 199, 385–392.
Blank, U., Seto, M.L., Adams, D.C., Wojchowski, D.M., Karolak, M.J., Oxburgh, L., 2008. An in vivo reporter of BMP signaling in organogenesis reveals targets in the developing kidney. BMC Dev. Biol. 8, 86.
Bouchard, M., Souabni, A., Mandler, M., Neubuser, A., Busslinger, M., 2002. Nephric lineage specification by Pax2 and Pax8. Genes Dev. 16, 2958–2970.
Brenner, B.M., Chertow, G.M., 1994. Congenital oligonephropathy and the etiology of adult hypertension and progressive renal injury. Am. J. Kidney Dis. 23, 171–175.
Brenner, B.M., Garcia, D.L., Anderson, S., 1988. Glomeruli and blood pressure. Less of one, more the other? Am. J. Hypertens 1, 335–347.
Brenner, B.M., Milford, E.L., 1993. Nephron underdosing: a programmed cause of chronic renal allograft failure. Am. J. Kidney Dis. 21, 66–72.
Brunskill, E.W., Aronow, B.J., Georgas, K., Rumballe, B., Valerius, M.T., Aronow, J., Kaimal, V., Jegga, A.G., Grimmond, S., McMahon, A.P., Patterson, L.T., Little, M.H., Potter, S.S., 2008. Atlas of gene expression in the developing kidney at microanatomic resolution. Dev. Cell 15, 781–791.
Carroll, T.J., Park, J.S., Hayashi, S., Majumdar, A., McMahon, A.P., 2005. Wnt9b plays a central role in the regulation of mesenchymal to epithelial transitions underlying organogenesis of the mammalian urogenital system. Dev. Cell 9, 283–292.
Cheng, H.T., Kim, M., Valerius, M.T., Surendran, K., Schuster-Gossler, K., Gossler, A., McMahon, A.P., Kopan, R., 2007. Notch2, but not Notch1, is required for proximal fate acquisition in the mammalian nephron. Development 134, 801–811.
Cheng, H.T., Kopan, R., 2005. The role of Notch signaling in specification of podocyte and proximal tubules within the developing mouse kidney. Kidney Int. 68, 1951–1952.

Cho, E.A., Patterson, L.T., Brookhiser, W.T., Mah, S., Kintner, C., Dressler, G.R., 1998. Differential expression and function of cadherin-6 during renal epithelium development. Development 125, 803–812.
Combes, A.N., Lesieur, E., Harley, V., Sinclair, A., Little, M.H., Wilhelm, D., Koopman, P., 2009. Three-dimensional visualization of testis cord morphogenesis, a novel tubulogenic mechanism in development. Dev. Dyn. 238, 1033–1041.
Dahl, U., Sjodin, A., Larue, L., Radice, G.L., Cajander, S., Takeichi, M., Kemler, R., Semb, H., 2002. Genetic dissection of cadherin function during nephrogenesis. Mol. Cell. Biol. 22, 1474–1487.
Davies, J., Lyon, M., Gallagher, J., Garrod, D., 1995. Sulphated proteoglycan is required for collecting duct growth and branching but not nephron formation during kidney development. Development 121, 1507–1517.
Dressler, G.R., 2006. The cellular basis of kidney development. Annu. Rev. Cell Dev. Biol. 22, 509–529.
Dressler, G.R., 2008. Another niche for Notch. Kidney Int. 73, 1207–1209.
Georgas, K., Rumballe, B., Wilkinson, L., Chiu, H.S., Lesieur, E., Gilbert, T., Little, M.H., 2008. Use of dual section mRNA in situ hybridisation/immunohistochemistry to clarify gene expression patterns during the early stages of nephron development in the embryo and in the mature nephron of the adult mouse kidney. Histochem. Cell Biol. 130, 927–942.
Hans, F., Dimitrov, S., 2001. Histone H3 phosphorylation and cell division. Oncogene 20, 3021–3027.
Hartwig, S., Hu, M.C., Cella, C., Piscione, T., Filmus, J., Rosenblum, N.D., 2005. Glypican-3 modulates inhibitory Bmp2-Smad signaling to control renal development in vivo. Mech. Dev. 122, 928–938.
Hoy, W.E., Bertram, J.F., Denton, R.D., Zimanyi, M., Samuel, T., Hughson, M.D., 2008. Nephron number, glomerular volume, renal disease and hypertension. Curr. Opin. Nephrol. Hypertens 17, 258–265.
Jacinto, A., Martinez-Arias, A., Martin, P., 2001. Mechanisms of epithelial fusion and repair. Nat. Cell Biol. 3, E117–E123.
Kispert, A., Vainio, S., McMahon, A.P., 1998. Wnt-4 is a mesenchymal signal for epithelial transformation of metanephric mesenchyme in the developing kidney. Development 125, 4225–4234.
Kobayashi, A., Kwan, K.M., Carrol, T.J., McMahon, A.P., Mendelsohn, C.L., Behringer, R.R., 2005. Distinct and sequential tissue-specific activities of the LIM-class homeobox gene Lim1 for tubular morphogenesis during kidney development. Development 132, 2809–2823.
Kobayashi, A., Valerius, M.T., Mugford, J.W., Carroll, T.J., Self, M., Oliver, G., McMahon, A.P., 2008a. Six2 defines and regulates a multipotent self-renewing nephron progenitor population throughout mammalian kidney development. Cell Stem Cell. 3, 169–181.
Kobayashi, T., Terada, Y., Kuwana, H., Tanaka, H., Okado, T., Kuwahara, M., Tohda, S., Sakano, S., Sasaki, S., 2008b. Expression and function of the Delta-1/Notch-2/Hes-1 pathway during experimental acute kidney injury. Kidney Int. 73, 1240–1250.
Kopan, R., Cheng, H.T., Surendran, K., 2007. Molecular insights into segmentation along the proximal–distal axis of the nephron. J. Am. Soc. Nephrol. 18, 2014–2020.
Kremer, J.R., Mastronarde, D.N., McIntosh, J.R., 1996. Computer visualization of three-dimensional image data using IMOD. J. Struct. Biol. 116, 71–76.
Kurima, K., Warman, M.L., Krishnan, S., Domowicz, M., Krueger, R.C., Deyrup, A., Schwartz, N.B., 1998. A member of a family of sulfate-activating enzymes causes murine brachymorphism (vol 95, pg 8681, 1998). Proc. Natl. Acad. Sci. U. S. A. 95, 12071.
Leimeister, C., Schumacher, N., Gessler, M., 2003. Expression of Notch pathway genes in the embryonic mouse metanephros suggests a role in proximal tubule development. Gene Expression Patterns 3, 595–598.
Little, M.H., Brennan, J., Georgas, K., Davies, J.A., Davidson, D.R., Baldock, R.A., Beverdam, A., Bertram, J.F., Capel, B., Chiu, H.S., Clements, D., Cullen-McEwen, L., Fleming, J., Gilbert, T., Herzlinger, D., Houghton, D., Kaufman, M.H., Kleymenova, E., Koopman, P.A., Lewis, A.G., McMahon, A.P., Mendelsohn, C.L., Mitchell, E.K., Rumballe, B.A., Sweeney, D.E., Valerius, M.T., Yamada, G., Yang, Y., Yu, J., 2007. A high-resolution anatomical ontology of the developing murine genitourinary tract. Gene Expression Patterns 7, 680–699.
Mackenzie, H.S., Tullius, S.G., Heemann, U.W., Azuma, H., Rennke, H.G., Brenner, B.M., Tilney, N.L., 1994. Nephron supply is a major determinant of long-term renal allograft outcome in rats. J. Clin. Invest. 94, 2148–2152.
Mah, S.P., Saueressig, H., Goulding, M., Kintner, C., Dressler, G.R., 2000. Kidney development in cadherin-6 mutants: delayed mesenchyme-to-epithelial conversion and loss of nephrons. Dev. Biol. 223, 38–53.
McCright, B., Gao, X., Shen, L., Lozier, J., Lan, Y., Maguire, M., Herzlinger, D., Weinmaster, G., Jiang, R., Gridley, T., 2001. Defects in development of the kidney, heart and eye vasculature in mice homozygous for a hypomorphic Notch2 mutation. Development 128, 491–502.
McCright, B., Lozier, J., Gridley, T., 2002. A mouse model of Alagille syndrome: Notch2 as a genetic modifier of Jag1 haploinsufficiency. Development 129, 1075–1082.
Mugford, J.W., Sipila, P., McMahon, J.A., McMahon, A.P., 2008. Osr1 expression demarcates a multi-potent population of intermediate mesoderm that undergoes progressive restriction to an Osr1-dependent nephron progenitor compartment within the mammalian kidney. Dev. Biol. 324, 88–98.
Nakai, S., Sugitani, Y., Sato, H., Ito, S., Miura, Y., Ogawa, M., Nishi, M., Jishage, K., Minowa, O., Noda, T., 2003. Crucial roles of Brn1 in distal tubule formation and function in mouse kidney. Development 130, 4751–4759.
Narlis, M., Grote, D., Gaitan, Y., Boualia, S.K., Bouchard, M., 2007. Pax2 and pax8 regulate branching morphogenesis and nephron differentiation in the developing kidney. J. Am. Soc. Nephrol. 18, 1121–1129.
Nawshad, A., 2008. Palatal seam disintegration: to die or not to die? That is no longer the question. Dev. Dyn. 237, 2643–2656.
Niehrs, C., 2006. Function and biological roles of the Dickkopf family of Wnt modulators. Oncogene 25, 7469–7481.
Nyengaard, J.R., Bendtsen, T.F., 1992. Glomerular number and size in relation to age, kidney weight, and body surface in normal man. Anat. Rec. 232, 194–201.
Osses, N., Gutierrez, J., Lopez-Rovira, T., Ventura, F., Brandan, E., 2006. Sulfation is required for bone morphogenetic protein 2-dependent Id1 induction. Biochem. Biophys. Res. Commun. 344, 1207–1215.
Oxburgh, L., Chu, G.C., Michael, S.K., Robertson, E.J., 2004. TGFbeta superfamily signals are required for morphogenesis of the kidney mesenchyme progenitor population. Development 131, 4593–4605.
Rumballe, B., Georgas, K., Little, M.H., 2008. High-throughput paraffin section in situ hybridization and dual immunohistochemistry on mouse tissues. CSH Protoc. 310.1101/pdb.prot5030.
Schmidt-Ott, K.M., Masckauchan, T.N., Chen, X., Hirsh, B.J., Sarkar, A., Yang, J., Paragas, N., Wallace, V.A., Dufort, D., Pavlidis, P., Jagla, B., Kitajewski, J., Barasch, J., 2007. Beta-catenin/TCF/Lef controls a differentiation-associated transcriptional program in renal epithelial progenitors. Development 134, 3177–3190.
Stark, K., Vainio, S., Vassileva, G., McMahon, A.P., 1994. Epithelial transformation of metanephric mesenchyme in the developing kidney regulated by Wnt-4. Nature 372, 679–683.
Sugahara, K., Schwartz, N.B., 1982. Defect in 3′-phosphoadenosine 5′-phosphosulfate synthesis in brachymorphic mice. 2. Tissue distribution of the defect. Arch. Biochem. Biophys. 214, 602–609.
Tetsu, O., McCormick, F., 1999. Beta-catenin regulates expression of cyclin D1 in colon carcinoma cells. Nature 398, 422–426.
Valerius, M.T., McMahon, A.P., 2008. Transcriptional profiling of Wnt4 mutant mouse kidneys identifies genes expressed during nephron formation. Gene Expression Patterns 8, 297–306.
Wilson, V.A., Gallagher, J.T., Merry, C.L., 2002. Heparan sulfate 2-O-sulfotransferase (Hs2st) and mouse development. Glycoconj. J. 19, 347–354.
Zaid, A., Roubtsova, A., Essalmani, R., Marcinkiewicz, J., Chamberland, A., Hamelin, J., Tremblay, M., Jacques, H., Jin, W., Davignon, J., Seidah, N.G., Prat, A., 2008. Proprotein convertase subtilisin/kexin type 9 (PCSK9): hepatocyte-specific low-density lipoprotein receptor degradation and critical role in mouse liver regeneration. Hepatology 48, 646–654.
Zavadil, J., Cermak, L., Soto-Nieves, N., Bottinger, E.P., 2004. Integration of TGF-beta/Smad and Jagged1/Notch signalling in epithelial-to-mesenchymal transition. EMBO J. 23, 1155–1165.